

Final report on "Joint Service Graduate Fellowship Program"

The graduate fellowship was first held by Dan Stamper-Kurn from October 1997 until his graduation on February 1, 2000 and then by Ananth Chikkatur from September 1, 2000 until October 14, 2001. The following papers were published by those two students during the time they were supported by the JSEP fellowship:

1. T.L. Gustavson, A.P. Chikkatur, A.E. Leanhardt, A. Görlitz, S. Gupta, D.E. Pritchard, and W. Ketterle:
Transport of Bose-Einstein Condensates with Optical Tweezers.
Phys. Rev. Lett. **88**, 020401 (2002).
2. A. Görlitz, J.M. Vogels, A.E. Leanhardt, C. Raman, T.L. Gustavson, J.R. Abo-Shaeer, A.P. Chikkatur, S. Gupta, S. Inouye, T. Rosenband, and W. Ketterle:
Realization of Bose-Einstein condensates in lower dimensions.
Phys. Rev. Lett. **87**, 130402 (2001).
3. S. Inouye, S. Gupta, T. Rosenband, A.P. Chikkatur, A. Görlitz, T.L. Gustavson, A.E. Leanhardt, D.E. Pritchard, and W. Ketterle:
Observation of vortex phase singularities in Bose-Einstein condensates.
Phys. Rev. Lett. **87**, 080402 (2001).
4. A. Görlitz, A.P. Chikkatur, and W. Ketterle:
Enhancement and suppression of spontaneous emission and light scattering by quantum degeneracy.
Phys. Rev. A **36**, 041601(R) (2001).
5. A.P. Chikkatur, A. Görlitz, D.M. Stamper-Kurn, S. Inouye, S. Gupta, and W. Ketterle:
Suppression and enhancement of impurity scattering in a Bose-Einstein condensate.
Phys. Rev. Lett. **85**, 483-486 (2000).
6. D.M. Stamper-Kurn and W. Ketterle:
Spinor Condensates and Light Scattering from Bose-Einstein Condensates.
in: *Coherent Atomic Matter Waves*, Les Houches Summer School Session LXXII in 1999, edited by R. Kaiser, C. Westbrook, and F. David (Springer, New York, 2001), pp. 137-217; e-print cond-mat/0005001.
7. J. Stenger, S. Inouye, D.M. Stamper-Kurn, A.P. Chikkatur, D.E. Pritchard, and W. Ketterle:
Bragg spectroscopy and superradiant Rayleigh scattering in a Bose-Einstein condensate.
Appl. Phys. B **69**, 347-352 (1999).
8. D.M. Stamper-Kurn, A.P. Chikkatur, A. Görlitz, S. Inouye, S. Gupta, D.E. Pritchard, and W. Ketterle:
Excitation of phonons in a Bose-Einstein condensate by light scattering.
Phys. Rev. Lett. **83**, 2876-2879 (1999).
9. S. Inouye, A.P. Chikkatur, D.M. Stamper-Kurn, J. Stenger, D.E. Pritchard, and W. Ketterle:
Superradiant Rayleigh scattering from a Bose-Einstein condensate.
Science **285**, 571-574 (1999).

10. D.M. Stamper-Kurn, H.-J. Miesner, A.P. Chikkatur, S. Inouye, J. Stenger, and W. Ketterle:
Quantum tunneling across spin domains in a Bose-Einstein condensate.
Phys. Rev. Lett. **83**, 661-665 (1999).
11. W. Ketterle, D.S. Durfee, and D.M. Stamper-Kurn:
Making, probing and understanding Bose-Einstein condensates.
In *Bose-Einstein condensation in atomic gases*, Proceedings of the International School of Physics "Enrico Fermi", Course CXL, edited by M. Inguscio, S. Stringari and C.E. Wieman (IOS Press, Amsterdam, 1999) pp. 67-176; e-print cond-mat/9904034.
12. J. Stenger, S. Inouye, A.P. Chikkatur, D.M. Stamper-Kurn, D.E. Pritchard, and W. Ketterle:
Bragg spectroscopy of a Bose-Einstein condensate.
Phys. Rev. Lett. **82**, 4569-4573 (1999).
13. H.-J. Miesner, D.M. Stamper-Kurn, J. Stenger, S. Inouye, A.P. Chikkatur, and W. Ketterle:
Observation of metastable states in spinor Bose-Einstein condensates.
Phys. Rev. Lett. **82**, 2228-2231 (1999).
14. J. Stenger, S. Inouye, M.R. Andrews, H.-J. Miesner, D.M. Stamper-Kurn, and W. Ketterle:
Strongly enhanced inelastic collisions in a Bose-Einstein condensate near Feshbach resonances.
Phys. Rev. Lett. **82**, 2422-2425 (1999).
15. M. Naraschewski and D.M. Stamper-Kurn:
Analytical description of a trapped semi-ideal Bose gas at finite temperature.
Phys. Rev. A **58**, 2423 (1998).
16. J. Stenger, D.M. Stamper-Kurn, M.R. Andrews, A.P. Chikkatur, S. Inouye, H.-J. Miesner, and W. Ketterle:
Optically confined Bose-Einstein condensates.
Proceedings of the Symposium on "Quantum Fluids and Solids" (QFS 98), Amherst, Massachusetts, June 9-14, 1998.
J. Low Temp. Phys. **113**, 167-188 (1998).
17. J. Stenger, S. Inouye, D.M. Stamper-Kurn, H.-J. Miesner, A.P. Chikkatur, and W. Ketterle:
Spin domains in ground state spinor Bose-Einstein condensates.
Nature **396**, 345-348 (1998).
18. D.M. Stamper-Kurn, H.-J. Miesner, A.P. Chikkatur, S. Inouye, J. Stenger, and W. Ketterle:
Reversible formation of a Bose-Einstein condensate.
Phys. Rev. Lett. **81**, 2194-2197 (1998).
19. S. Inouye, M.R. Andrews, J. Stenger, H.-J. Miesner, D.M. Stamper-Kurn, and W. Ketterle:
Observation of Feshbach resonances in a Bose-Einstein condensate.
Nature **392**, 151-154 (1998).
20. D.M. Stamper-Kurn, H.-J. Miesner, S. Inouye, M.R. Andrews, and W. Ketterle:
Collisionless and hydrodynamic excitations of a Bose-Einstein condensate.
Phys. Rev. Lett. **81**, 500-503 (1998).

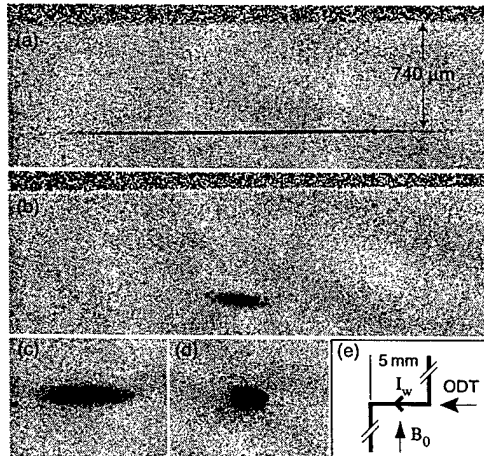
21. H.-J. Miesner, D.M. Stamper-Kurn, M.R. Andrews, D.S. Durfee, S. Inouye, and W. Ketterle:
Bosonic stimulation in the formation of a Bose-Einstein condensate.
Science **279**, 1005-1007 (1998).
22. D.M. Stamper-Kurn, M.R. Andrews, A.P. Chikkatur, S. Inouye, H.-J. Miesner, J. Stenger, and W. Ketterle:
Optical confinement of a Bose-Einstein condensate.
Phys. Rev. Lett. **80**, 2027-2030 (1998).

Here is a summary of the work done by the supported students:

1. Transport of Bose-Einstein Condensates with Optical Tweezers

Conventional condensate production techniques severely limit optical and mechanical access to experiments due to the many laser beams and magnetic coils needed to create BECs. This conflict between cooling infrastructure and accessibility to manipulate and study condensates has been a major restriction to previous experiments. So far, most experiments were carried out within a few millimeters of where the condensate was created. What is highly desirable is a condensate “beam line” that delivers condensates to a variety of experimental platforms.

We have transported gaseous Bose-Einstein condensates over distances up to 44 cm [1]. This was accomplished by trapping the condensate in the focus of an infrared laser and translating the location of the laser focus with controlled acceleration. Condensates of order 10^6 atoms were moved into an auxiliary “science” chamber which has excellent optical and mechanical access. This technique is ideally suited to deliver condensates close to surfaces, e.g., to microscopic waveguides and into electromagnetic cavities. As a proof-of-principle demonstration, we have used the tweezers technique to transfer condensates into a magnetic trap formed by a Z-shaped wire suspended in the science chamber. The same procedure can now be used to load condensates into atom chips. In such devices, patterns of wires are lithographically deposited on a surface and may allow the realization of single-mode waveguides and atom interferometers.



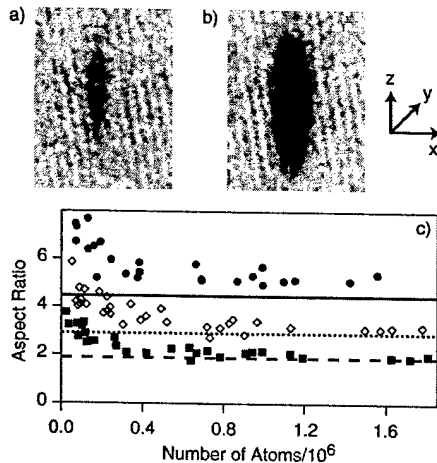
Absorption images of condensates in the science chamber, side view. All images have the same scale. Condensates of $\approx 6 \cdot 10^5$ atoms are shown in (a) optical trap and (b) wire-trap. The center segment of the Z-shaped wire is visible as a dark speckled horizontal strip and is $740 \mu\text{m}$ above the trapped atoms. The condensate was released from (c) an optical trap after 10 msec time of flight and (d) wiretrap after 23 ms time of flight. (e) Schematic of the wiretrap, top view. $I_w = 2 \text{ A}$ is the current through the wire, and $B_0 = 2.9 \text{ G}$ is the bias field. Atoms are trapped below the 5-mm-long central segment of the wire, which is aligned with the optical trap axis. The wiretrap was located 36 cm from where the condensates were produced.

2. Realization of Bose-Einstein condensates in lower dimensions

Bose-Einstein condensates of sodium atoms have been prepared in optical and magnetic traps in which the energy-level spacing in one or two dimensions exceeds the interaction energy between atoms. This realized condensates of lower dimensionality [2]. In anisotropic traps, a primary indicator of crossing the transition temperature for Bose-Einstein condensation is a sudden change of the aspect ratio of the ballistically expanding cloud. The transition to lower dimensions is a smooth cross-over, but has similar

indicators. In the 3D Thomas-Fermi limit the degree of anisotropy of a BEC is independent of the number N of atoms, whereas in 1D and 2D, the aspect ratio depends on N . This was used in our experiments as a distinctive feature of lower dimensionality.

In our traps, the ratio of the highest to lowest frequency was about 100. Due to this extreme geometry the number of atoms at the cross-over to lower-dimensionality was rather large ($> 10^5$ in the 2D case) which provides a good starting point for the exploration of phenomena which only occur in one or two dimensions.



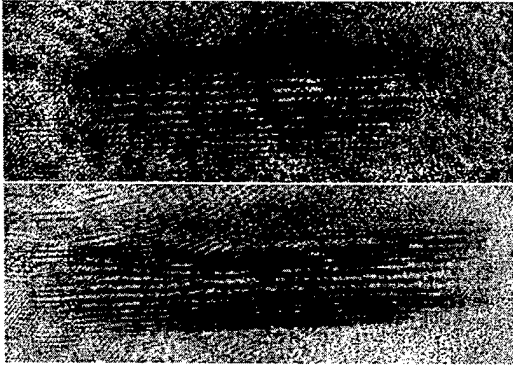
Cross-over from 3D to 2D condensates observed in the change of the aspect ratio. Condensates were released from a disk-shaped optical trap and observed after 15 ms time-of-flight. a) (2D) condensate with 9×10^4 atoms b) (3D) condensate with 8×10^5 atoms in a trap with vertical trap frequency of 790 Hz. c) Aspect ratio as a function of atom number for optical traps with vertical trap frequencies of 1620 Hz (filled circles), 790 Hz (open diamonds) and 450 Hz (filled squares). The lines indicate the aspect ratios as expected for condensates in the 3D (Thomas-Fermi) regime. We attribute discrepancies between expected and measured aspect ratio for large numbers to the influence of anharmonicities on the measurement of the trap frequencies.

3. Observation of vortex phase singularities in Bose-Einstein condensates

Bose-Einstein condensates of dilute atomic gases offer a unique opportunity to study quantum hydrodynamics. The low density of the gas allows direct comparison with first principle theories.

Recently, vortices in a Bose-Einstein condensate have been realized experimentally and are currently under intensive study [3-5]. In most of this work, vortices were identified by observing the density depletion at the cores. The velocity field was inferred only indirectly, with the exception of the work on circulation in a two-component condensate [3]. The flow field of a vortex can be directly observed when the phase of the macroscopic wavefunction is measured using interferometric techniques. In our work, we created one or several vortices in one condensate by moving a laser beam through it and imaged its phase by interfering it with a second unperturbed condensate which served as a local oscillator [6].

The characteristic signature of vortices were dislocations in the interference fringes. The "extra" fringe which terminates at the vortex core corresponds to one quantum of circulation h/m (where m is the atomic mass and h Planck's constant) or a phase change of 2π integrated along a path around the vortex core.



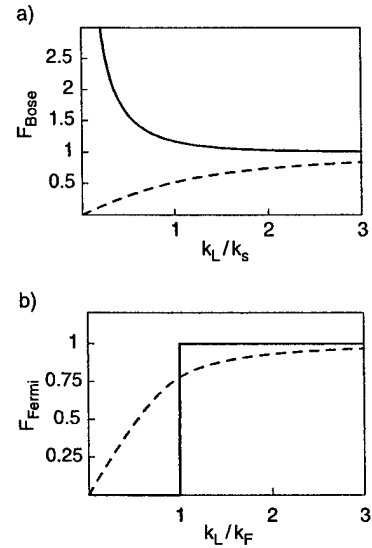
Observation of the phase singularities of vortices created by sweeping a laser beam through a condensate. Without the sweep, straight fringes of about $20\ \mu\text{m}$ spacings were observed (upper image), while after the sweep, fork-like dislocations appeared (lower image). The speed of the sweep was $1.1\ \mu\text{m/ms}$ corresponding to a Mach number of 0.1. The field of view of each image is $1.1\ \text{mm} \times 0.38\ \text{mm}$.

4. Enhancement and suppression of spontaneous emission and light scattering by quantum degeneracy

Quantum degeneracy modifies light scattering and spontaneous emission. For fermions, Pauli blocking leads to a suppression of both processes. In contrast, in a weakly interacting Bose-Einstein condensate, we found spontaneous emission to be enhanced, while light scattering is suppressed [7]. This difference is attributed to many-body effects and quantum interference in a Bose-Einstein condensate.

Generally, transition rates between an initial state with population N_1 and a final state with population N_2 are proportional to $N_1(1+N_2)$ for bosons and to $N_1(1-N_2)$ for fermions. This simple derivation of transition rates using occupation numbers becomes subtle or even invalid for correlated many-body states such as an interacting Bose-Einstein condensate ground state. We analyzed under which circumstances the simple approach can be used to reproduce the correct results for the interaction between light and a BEC. We showed theoretically that spontaneous emission in a weakly interacting BEC is enhanced, consistent with the description using occupation numbers, and calculated the enhancement factor. We compared this result to light scattering in a BEC, which is suppressed due to many-body interference effects not included in the simple derivation, as we have shown experimentally and theoretically in previous work [8]. In contrast, in fermionic systems quantum degeneracy leads to a suppression of *both* spontaneous emission and light scattering.

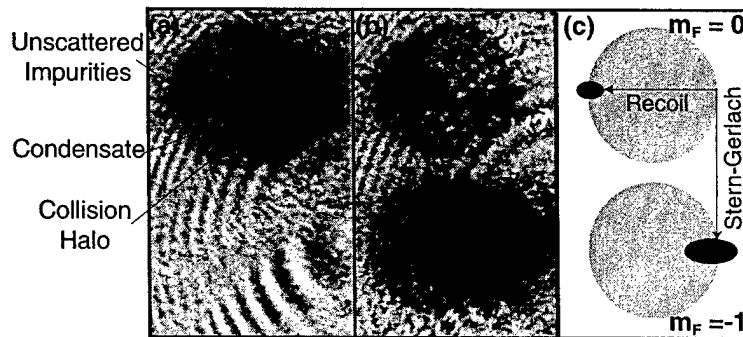
Modification of spontaneous emission (solid line) and light scattering (dashed line) due to quantum degeneracy. In (a) we have plotted the enhancement factor for spontaneous emission and the suppression factor for light scattering for a weakly interacting Bose-Einstein condensate as a function of the light wave vector k_L in units of k_s , the wave vector of an atom moving at the speed of sound. In (b) the suppression factors for spontaneous emission and light scattering in a Fermi gas at zero temperature are plotted as a function of k_L in units of the Fermi wave vector k_F .



5. Superfluid suppression of impurity scattering in a Bose-Einstein condensate

The concept of superfluidity applies to both macroscopic and microscopic objects. In both cases, there is no dissipation or drag force as long as the objects move with a velocity less than the so-called critical velocity. A moving macroscopic object creates a complicated flow field. Above a certain velocity, vortices are created. In contrast, the physics of moving impurities, which are microscopic objects, is much simpler. At velocities larger than the Landau critical velocity, they will create elementary excitations, phonons or rotons in the case of liquid helium-4.

We could create impurity atoms in a trapped BEC by transferring some of the atoms into another hyperfine state using an optical Raman transition. The photon recoil and therefore the velocity of the impurity atoms was varied by the angle between the two laser beams. Collisions between the impurity atoms and the condensate were observed as a redistribution of momentum when the velocity distribution was analyzed with a ballistic expansion technique. The collisional cross section was dramatically reduced when the velocity of the impurities was reduced below the speed of sound of the condensate, in agreement with the Landau criterion for superfluidity [9].

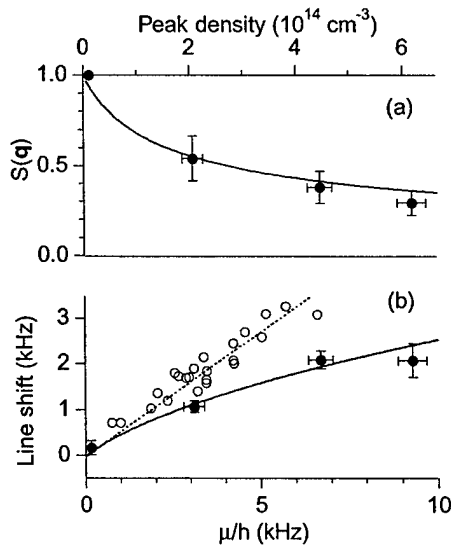


Observation of collisions between the condensate and impurities. The impurities in the $m=0$ hyperfine state traveled at 6 cm/s to the left. Collisions redistribute the momentum over a sphere in momentum space, resulting in the observed halo (a). In figure (b), the impurities and the condensate in the $m=-1$ state were separated with a magnetic field gradient during the ballistic expansion. The effect of collisions is to slow down some of the impurity atoms and speed up the condensate atoms. The absorption images are 4.5 mm times 7.2 mm in size.

6. Excitation of phonons in a Bose-Einstein condensate by light scattering

Light scattering imparts momentum to the condensate and creates an excitation (which can be a phonon or a free particle). A detailed study of the scattered light should therefore reveal a detailed picture of the Bose condensate similar to the case of superfluid helium where neutron scattering was used to obtain the spectrum of elementary excitations.

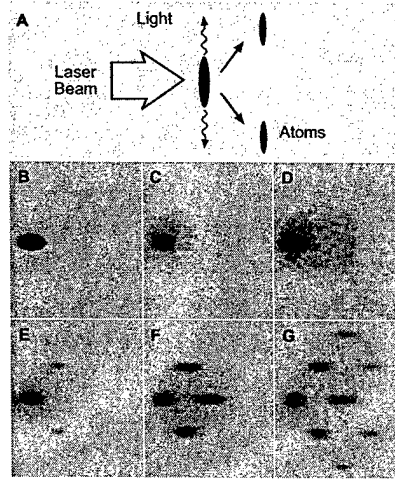
In previous work [10] we showed how a condensate responds to a large momentum transfer which lead to particle-like excitations. Light scattering at small angles does not impart enough momentum to the condensate to create a recoiling atom. Instead, it creates a sound wave by “optically imprinting” phonons into the gas. A sound wave is a collective excitation of all the atoms in the system and therefore requires that the atoms don’t act as individual atoms, but show correlated motion. It has been predicted that this correlated motion results in much weaker light scattering than for free atoms. We found a significant decrease of the rate of light scattering in the phonon regime, providing dramatic evidence for the presence of correlated momentum excitations in the many-body condensate wavefunction [8]. For high-density condensates, even large-angle scattering is in the phonon regime. Therefore, this effect should turn a “pitch-black” condensate transparent since the collective nature of the condensate suppresses its ability to scatter light.



(a) Static structure factor $S(q)$ and (b) shift of the line center from the free particle resonance. $S(q)$ characterizes the strength of the scattering process during which momentum q is transferred to the condensate. As the density and the chemical potential μ increase, the structure factor is reduced, and the Bragg resonance is shifted upward in frequency. Solid lines are predictions of a local-density approximation. Dotted line indicates a mean-field shift of $4\mu/7\hbar$ as measured in the free-particle regime (shown in open symbols).

7. Superradiant Rayleigh scattering from a Bose-Einstein condensate

We have discovered a new phenomenon in the scattering of light by a condensate: highly directional, “superradiant” scattering of light and atoms [11]. This phenomenon is deeply rooted in the long coherence time of a condensate. When a condensate has scattered light, an imprint is left in the form of long-lived excitations. This “memory” accelerates the scattering of further photons into the same directions. It provides a gain mechanism for the generation of directed beams of atoms and light.



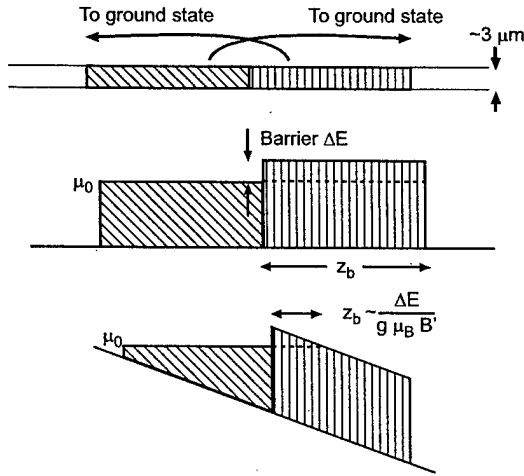
Observation of superradiant Rayleigh scattering. (a) A cigar-shaped condensate is illuminated with a single off-resonant laser beam. Collective scattering leads to photons scattered predominantly along the axial direction, and atoms at 45 degrees. (b-g) Absorption images after 20 ms time-of-flight show the atomic momentum distribution after exposure of the atoms to a laser pulse of variable duration. When the polarization is parallel to the long axis, superradiance is suppressed, and normal Rayleigh scattering was observed (b-d). For perpendicular polarization, directional superradiant scattering of atoms was observed (e-g), and evolved to repeated scattering for longer laser pulses (f,g). The pulse durations are 25 μ s (b), 100 μ s (c,d), 35 μ s (e), 75 μ s (f), 100 μ s (g). The field of view of each image is 2.8 mm x 3.3 mm. The scattering angle appears to be larger than 45 degrees due to the angle of observation. All images use the same gray scale except for (d), which enhances the small signal of Rayleigh scattered atoms in (c).

This phenomenon is fairly dramatic. When a condensate was illuminated with a single weak laser beam, it randomly scattered light into all directions (with the well-known dipolar pattern – this is ordinary Rayleigh scattering). However, above a certain threshold intensity, the condensate produced two highly directional beams of light. Such highly directional light scattering was accompanied by the production of highly directional beams of recoiling atoms (see figure). These beams of atoms were shown to build up by matter wave amplification. The condensate acted as an amplifier for a recoiling atom and “amplified” it to about a million atoms. If one had collected the light in an optical cavity, one would have realized an optical laser. Therefore, the simultaneous superradiant emission of light and atoms emphasizes the symmetry between atom lasers and optical lasers.

8. Quantum tunneling across spin domains in a Bose-Einstein condensate

The observation of metastable spin domains in optically trapped $F=1$ spinor Bose-Einstein condensates of sodium [12] raised the question of how thermal equilibrium would ultimately be achieved. Besides thermally activated processes we observed quantum tunneling as equilibration process. For the study of this process, spinor condensates were prepared which consisted of only two spin domains in the $m_F=0$ and $m_F=+1$ states. Those domains are immiscible due to their antiferromagnetic interaction. When a field gradient was added which made it energetically favorable for the two domains to change sides, quantum tunneling was observed. A mean-field description of the tunneling process was developed and agreed well with the measurements [13].

The analysis showed that the tunneling rates are a sensitive probe of the boundary between spin domains, and indicated an unpredicted spin structure in the boundary between spin domains which is prohibited in the bulk fluid.



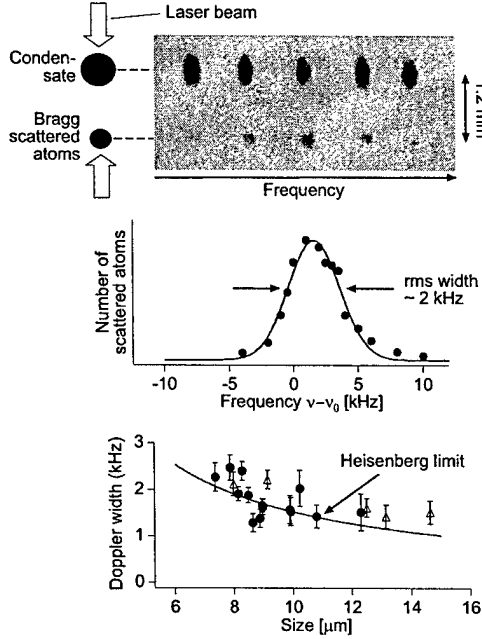
Study of quantum tunneling in a two-component Bose-Einstein condensate. The $m_F=1$ and $m_F=0$ (vertical hatch) atoms form two immiscible spin domains (upper figure) because the $m_F=1$ atoms experience an energy barrier due to the repulsive mean field interaction (middle figure). When a longitudinal magnetic field gradient is applied, the effective potential for the $m_F=1$ atoms changes to the lower figure, and the spin domains can rearrange themselves by quantum tunneling through each other.

9. Bragg spectroscopy of a Bose-Einstein condensate

The first evidence for Bose-Einstein condensation in dilute gases was obtained by a sudden narrowing of the velocity distribution as observed for ballistically expanding clouds of atoms. However, the dominant contribution to the observed momentum distribution of the expanding condensate was the released interaction energy (mean-field energy) resulting in momentum distributions much broader than the zero-point motion of the ground state of the harmonic trapping potential. Since the size of a trapped condensate with repulsive interactions is larger than the trap ground state, the momentum distribution should be considerably narrower than in the trap ground state. We could measure the momentum distribution of a trapped condensate with Doppler velocimetry using two-photon Bragg scattering. We observed that the momentum distribution was Heisenberg uncertainty limited by its finite size, i.e. the coherence length of the condensate was equal to its size [10].

A shift of the narrow Bragg resonance was caused by the repulsive interactions within the condensate resulting in a spectroscopic measurement of the mean-field energy. More

generally, we have established Bragg scattering as a spectroscopic technique to probe properties of the condensate. It can be used to map out the density fluctuations of the system and thus to measure directly the dynamic structure factor $S(q, \omega)$, which is the Fourier transform of the density-density correlation function and is central to the theoretical description of many-body systems.



Bragg spectroscopy of a trapped condensate. A condensate was exposed to two counterpropagating laser beams and analyzed using time of flight absorption imaging (upper part). The number of Bragg scattered atoms showed a narrow resonance when the difference frequency between the two laser beams was varied (upper and middle part). The width of the resonance was studied for various radial sizes of the condensate. The solid line (lower part) compares the experimental results with the prediction for the momentum uncertainty due to the finite size.

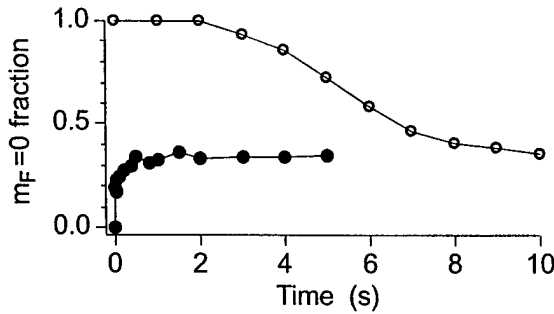
10. Metastable Bose-Einstein condensates

During the studies of the spinor ground states we encountered two different types of metastability which we investigated in more detail [12]. In one case, a two-component condensate in the $m_F = +1, 0$ hyperfine states was stable in spin composition, but spontaneously formed a metastable spatial arrangement of spin domains. In the other, a single component $m_F = 0$ condensate was metastable in spin composition with respect to the development of $m_F = +1, -1$ ground-state spin domains. In both cases, the energy barriers which caused the metastability were much smaller than the temperature of the gas (as low as 0.1 nK compared to 100 nK) which would suggest a rapid thermal relaxation. However, since the thermal energy is only available to non-condensed atoms, this thermal relaxation was slowed considerably due to the high condensate fraction and the extreme diluteness of the non-condensed cloud.

When a condensate was initially prepared in a pure $m_F = 0$ state metastability of up to 5 sec was observed for the formation of the equilibrium spin domain structure (see figure). In contrast when the system was prepared in an equal mixture of $m_F = +1$ and $m_F = -1$ atoms the fraction of atoms in the $m_F = 0$ state grew without delay, arriving at equilibrium within just 200 ms.

Metastability of the spatial distribution was observed in a system of $m_F = +1$ and $m_F = 0$ atoms. After the $m_F = 0$ state was populated with an rf pulse, the system rapidly developed

into alternating layers of $m_F=0$ and $m_F=1$ spin domains of about $40\text{ }\mu\text{m}$ in thickness which were metastable for 20 seconds in the absence of magnetic field gradients.



Metastability of the pure $m_F = 0$ state in the presence of a magnetic bias field (250 mG) and gradient (44 mG/cm). The evolution toward equilibrium of an initially pure $m_F = 0$ condensate (open symbols), and a mixture of $m_F = 1$ and $m_F = -1$ (closed symbols) is shown by plotting the fraction of atoms in the $m_F = 0$ state vs. dwell time in the optical trap.

11. Strongly enhanced inelastic collisions in a Bose-Einstein condensate near Feshbach resonances

The properties of Bose-Einstein condensed gases can be strongly altered by tuning the external magnetic field near a Feshbach resonance. Feshbach resonances affect elastic collisions and lead to the observed modification of the scattering length. However, we found that this is accompanied by a strong increase in the rate of inelastic collisions. The observed three-body loss rate increased when the scattering length was tuned to both larger or smaller values than the off-resonant value [14]. The maximum measured increase of the loss rate was several orders of magnitude. Sweeps of the magnetic field through the resonance resulted in loss of most of the atoms in one microsecond. These observations are not explained by theoretical treatments and indicate molecular and many-body physics which is not yet accounted for. The strong losses impose severe limitations for using Feshbach resonances to tune the properties of Bose-Einstein condensates. A new Feshbach resonance in sodium at 1195 G was observed which has a region of negative scattering length on the low field side of the resonance which can therefore be directly approached without crossing any other resonance.

12. Analytical description of a trapped semi-ideal Bose-Gas

One focus of research on dilute gas Bose-Einstein condensates is the study of thermodynamic quantities such as the transition temperature to Bose-Einstein condensation, and the condensate fraction. In particular, for the dilute gas Bose condensates, the weak interactions between particles and their low density allows for an accurate theoretical description of the effect of interactions in a many-body system starting from a microscopic understanding of two-particle collisions. In collaboration with Martin Naraschewski, a member of our group (DMS-K) explored the effect of interactions on a trapped partially condensed gas using an intuitive and accessible description of the interactions between the condensed and non-condensed atoms [15]. In this "semi-ideal" picture, interactions between condensed atoms are treated by the simple and verified Thomas-Fermi approximation, while the non-condensed fraction is treated as an ideal gas for which the trapping potential and the chemical potential are altered by repulsion from the condensate. This led to analytical expressions for the condensate

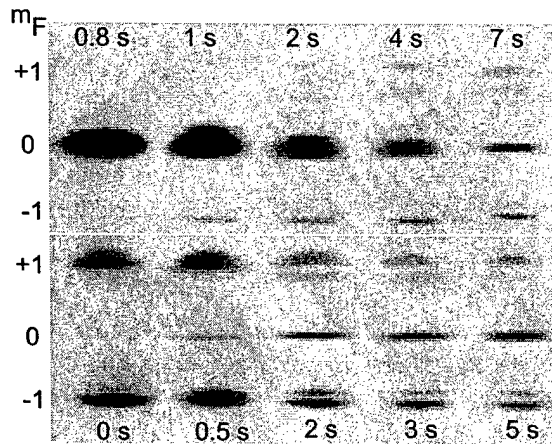
fraction and for the density of the trapped gas, which can be used directly in the comparison between theory and experimental data.

13. Spinor Bose-Einstein condensates in optical traps

We have studied the equilibrium state of spinor condensates in an optical trap [16]. In contrast to magnetically trapped condensates, spinor condensates have the orientation of the spin as a degree of freedom, which can be described by a multi-component wavefunction (one for each magnetic sublevel). In an $F=1$ spinor condensate subject to spin relaxation, two $m_F=0$ atoms can collide and produce a $m_F=1$ and a $m_F=-1$ atom and vice versa. The most dramatic effect was seen when we started with a condensate in a pure $m_F=0$ state. Depending on the external magnetic field, the formation of three domains of $m_F = +1, 0, -1$ atoms was observed.

The figure shows a sequence of images with different dwell times in the optical trap. Starting with either the pure $m_F=0$ component (upper series) or with a 50-50 mixture of the $m_F = \pm 1$ components (lower series), the same equilibrium distribution was reached.

Comparison of such equilibrium distributions to a theoretical model revealed that the spin-dependent interaction $c\vec{F}_1 \cdot \vec{F}_2$ between two sodium atoms in the $F=1$ state is anti-ferromagnetic (i.e. $c > 0$). Furthermore, the experimental results showed clear evidence for the miscibility of $m_F = -1$ and $m_F = +1$ components and the immiscibility of $m_F = \pm 1$ and $m_F = 0$. This opens the possibility for detailed studies of miscible and immiscible multi-component condensates.



Absorption images of spinor condensates released from the optical trap, after 25 ms of ballistic expansion. The different m_F states were separated by an axial field gradient (Stern-Gerlach filter). The images taken after various dwell times in the trap show how the atoms evolved into the same equilibrium distribution although they were initially prepared in a pure $m_F = 0$ state (upper row) or in equally populated $m_F = \pm 1$ states (lower row). The height of the images is 2.7 mm.

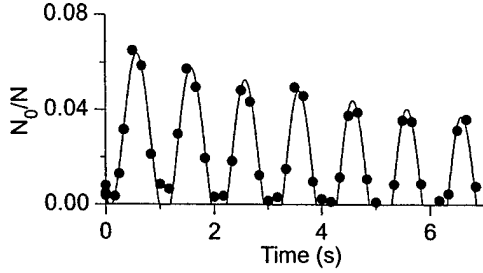
14. Reversible formation of a Bose-Einstein condensate

In an ordinary cryostat, the experimenter can raise and lower the temperature of a sample reversibly. In contrast, evaporative cooling is irreversible due to the loss of the evaporated atoms. Even if the temperature is raised again by (internal or external) heating of the sample, the number of atoms lost during the cooling stage cannot be recovered.

In recent experiments, we could cross the BEC transition reversibly by slowly changing the shape of the trapping potential using a combination of magnetic and optical

forces [17]. This process conserves entropy while changing the local phase space density.

By ramping up the power of an infrared beam focused into the center of the magnetic trap, we could increase the phase-space density by a factor of 50. The reversibility of crossing the BEC phase transition was demonstrated by preparing a magnetically trapped cloud just above the critical temperature and then sinusoidally modulating the infrared power. We could reversibly cycle at least 15 times back and forth across the BEC transition.

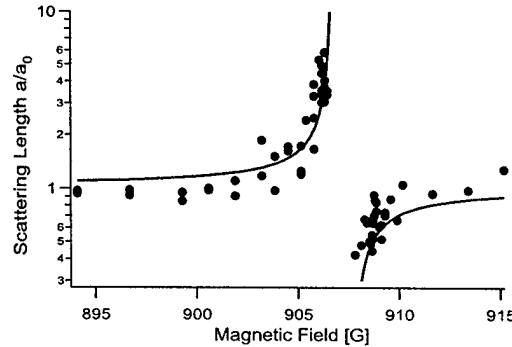


Adiabatic cycling through the phase transition by sinusoidally modulating the optical trapping potential. Shown is the condensate fraction versus time. The solid lines are guides to the eye.

15. Observation of Feshbach resonances in a Bose-Einstein condensate

All the essential properties of Bose condensed systems - the formation and shape of the condensate, the nature of its collective excitations and statistical fluctuations, the formation and dynamics of solitons and vortices - are determined by the strength of the atomic interactions. In atomic gases, the strength of the interaction, characterized by the scattering length, varies dispersively near a Feshbach resonance which occurs at a specific value of the external magnetic field.

Our recent observation of Feshbach resonances in an optically trapped condensate [18] was the first such observation for cold atoms. The strength of the interaction was inferred from the measured release energy. The figure clearly displays the predicted dispersive shape and shows evidence for a variation in the scattering length by more than a factor of ten. Our observation of the dispersive variation of the scattering length confirms the theoretical predictions about “tunability” of the scattering length with the prospect of “designing” atomic quantum gases with novel properties.

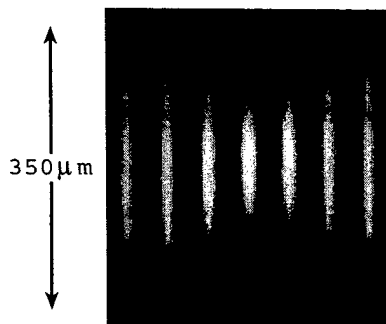


Observation of the Feshbach resonance at a magnetic field of 907 G using time-of-flight absorption imaging. The figure shows the normalized scattering length versus external magnetic field, together with the predicted shape.

16. Sound at non-zero temperature: collisionless and hydrodynamic excitations of a Bose-Einstein condensate

Collective excitations are the fingerprints of a system and reveal many of its dynamic properties. We extended earlier work on collective excitations of a Bose-Einstein condensate by studying them at non-zero temperature and at high density where they become analogous to first and second sound in superfluid helium [19]. The existence of such two modes is characteristic of a superfluid system.

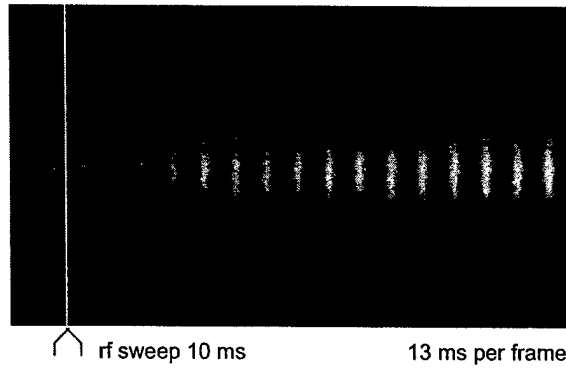
Our study focused on the lowest-lying shape oscillation. This oscillation was probed above and below the Bose-Einstein condensation temperature. The temperature dependencies of the frequency and damping rates of condensate oscillations indicate significant interactions between the condensate and the thermal cloud. First sound, which constitutes hydrodynamic oscillations of the thermal cloud, was observed. An antisymmetric dipolar oscillation of the thermal cloud and the condensate was also studied. This excitation represents the bulk flow of a superfluid through the normal fluid and has similarities to second sound. The detailed theoretical description of these results is currently a challenge for many-body theorists.



In situ images of the $m=0$ quadrupolar condensate oscillation near 30 Hz. A Bose-Einstein condensate with no discernible thermal component was imaged every 5 ms by phase-contrast imaging. The evident change in the axial length of the condensate was used to characterize the oscillation.

17. Bosonic stimulation in the formation of a Bose-Einstein condensate

Quantum-mechanical symmetry leads to bosonic stimulation, i.e. the probability of non-condensed atoms scattering into the condensate is proportional to the number of condensed atoms already present. This process is analogous to stimulated emission of photons and can be considered as “matter wave amplification.” When we observed the formation of the condensate after suddenly quenching the cloud below the transition temperature we obtained evidence for bosonic amplification [20]. Bosonic stimulation leads to an acceleration of the rate at which atoms enter the condensate - the formation process therefore starts slowly, speeds up and then approaches equilibrium.

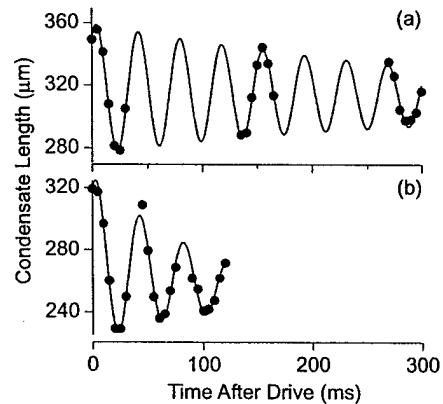


The formation of a Bose-Einstein condensate. Shown is a sequence of 18 phase-contrast images taken in situ of the same condensate. The first two frames show a thermal cloud at a temperature above the transition temperature. The following 16 frames were taken after the cloud was quenched below the BEC transition, and show the growth of a condensate at the center of the cloud at 13 ms intervals. Note the decrease in the number of thermal atoms and their smaller width after the rf sweep. The bright gray levels mark the high column density of the condensate. The length of the images is 630 μm .

18. All-optical confinement of a Bose-Einstein condensate

Magnetic confinement of Bose-Einstein condensates is incompatible with many precision measurements and applications in atom optics. Therefore, we realized an optical trap for a Bose-Einstein condensate [21]. It uses a single, focused infrared laser beam of only a few milliwatts of laser power, which is sufficient due to the very low energy of Bose condensates. In this trap, we have observed high atomic densities which were unprecedented both for Bose condensates and for optically trapped atoms. Furthermore, the trap works at arbitrary magnetic fields and for atoms in all hyperfine states. This has led to the observation of Feshbach resonances and spinor condensates. The optical trap may also serve as an “optical tweezers” to move condensates, and for example, place them close to surfaces and in optical and microwave cavities.

Damped quadrupolar condensate oscillations at low (a) and high (b) temperature. Points show the axial condensate length determined from fits to phase-contrast images (such as shown in the figure above). The oscillation at high temperature has a slightly lower frequency, and is damped more rapidly than at low temperature.



1. T.L. Gustavson, A.P. Chikkatur, A.E. Leanhardt, A. Görlitz, S. Gupta, D.E. Pritchard, and W. Ketterle, Phys. Rev. Lett. **88**, 020401 (2002).
2. A. Görlitz, J.M. Vogels, A.E. Leanhardt, C. Raman, T.L. Gustavson, J.R. Abo-Shaeer, A.P. Chikkatur, S. Gupta, S. Inouye, T. Rosenband, and W. Ketterle, Phys. Rev. Lett. **87**, 130402 (2001).

3. M.R. Matthews, B.P. Anderson, P.C. Haljan, D.S. Hall, C.E. Wieman, and E.A. Cornell, *Phys. Rev. Lett.* **83**, 2498 (1999).
4. K.W. Madison, F. Chevy, W. Wohlleben, and J. Dalibard, *Phys. Rev. Lett.* **84**, 806 (2000).
5. J.R. Abo-Shaeer, C. Raman, J.M. Vogels, and W. Ketterle, *Science* **292**, 476 (2001).
6. S. Inouye, S. Gupta, T. Rosenband, A.P. Chikkatur, A. Görlitz, T.L. Gustavson, A.E. Leanhardt, D.E. Pritchard, and W. Ketterle, *Phys. Rev. Lett.* **87**, 080402 (2001).
7. A. Görlitz, A.P. Chikkatur, and W. Ketterle, *Phys. Rev. A* **36**, 041601(R) (2001).
8. D.M. Stamper-Kurn, A.P. Chikkatur, A. Görlitz, S. Inouye, S. Gupta, D.E. Pritchard, and W. Ketterle, *Phys. Rev. Lett.* **83**, 2876 (1999).
9. A.P. Chikkatur, A. Görlitz, D.M. Stamper-Kurn, S. Inouye, S. Gupta, and W. Ketterle, *Phys. Rev. Lett.* **85**, 483 (2000).
10. J. Stenger, S. Inouye, A.P. Chikkatur, D.M. Stamper-Kurn, D.E. Pritchard, and W. Ketterle, *Phys. Rev. Lett.* **82**, 4569 (1999).
11. S. Inouye, A.P. Chikkatur, D.M. Stamper-Kurn, J. Stenger, D.E. Pritchard, and W. Ketterle, *Science* **285**, 571 (1999).
12. H.-J. Miesner, D.M. Stamper-Kurn, J. Stenger, S. Inouye, A.P. Chikkatur, and W. Ketterle, *Phys. Rev. Lett.* **82**, 2228 (1999).
13. D.M. Stamper-Kurn, H.-J. Miesner, A.P. Chikkatur, S. Inouye, J. Stenger, and W. Ketterle, *Phys. Rev. Lett.* **83**, 661 (1999).
14. J. Stenger, S. Inouye, M.R. Andrews, H.-J. Miesner, D.M. Stamper-Kurn, and W. Ketterle, *Phys. Rev. Lett.* **82**, 2422 (1999).
15. M. Naraschewski and D.M. Stamper-Kurn, *Phys. Rev. A* **58**, 2423 (1998).
16. J. Stenger, S. Inouye, D.M. Stamper-Kurn, H.-J. Miesner, A.P. Chikkatur, and W. Ketterle, *Nature* **396**, 345 (1998).
17. D.M. Stamper-Kurn, H.-J. Miesner, A.P. Chikkatur, S. Inouye, J. Stenger, and W. Ketterle, *Phys. Rev. Lett.* **81**, 2194 (1998).
18. S. Inouye, M.R. Andrews, J. Stenger, H.-J. Miesner, D.M. Stamper-Kurn, and W. Ketterle, *Nature* **392**, 151 (1998).
19. D.M. Stamper-Kurn, H.-J. Miesner, S. Inouye, M.R. Andrews, and W. Ketterle, *Phys. Rev. Lett.* **81**, 500 (1998).
20. H.-J. Miesner, D.M. Stamper-Kurn, M.R. Andrews, D.S. Durfee, S. Inouye, and W. Ketterle, *Science* **279**, 1005 (1998).
21. D.M. Stamper-Kurn, M.R. Andrews, A.P. Chikkatur, S. Inouye, H.-J. Miesner, J. Stenger, and W. Ketterle, *Phys. Rev. Lett.* **80**, 2027 (1998).

ATTACHMENT NUMBER 1

REPORTS AND REPORT DISTRIBUTION

REPORT TYPES

- (a) Performance (Technical) Report(s) (Include letter report(s)) Frequency: Annual
- (b) Final Technical Report, issued at completion of Grant.
NOTE: Final Technical Reports must have a SF-298 accompanying them. Unless otherwise stated in the grant, complete Block 12a. of the SF-298: "Approved for Public Release; distribution is Unlimited."
- (c) Final Financial Status Report (SF 269)
- (d) Final Patent Report (DD 882)

REPORTS DISTRIBUTION		
ADDRESSEES	REPORT TYPES	NUMBER OF COPIES
Office of Naval Research Program Officer Colin E. Wood ONR 312 Ballston Centre Tower One 800 North Quincy Street Arlington, VA 22217-5660	(a) & (b) w/(SF-298's)	3
Administrative Grants Officer OFFICE OF NAVAL RESEARCH REGIONAL OFFICE BOSTON 495 SUMMER STREET ROOM 103 BOSTON, MA 02210-2109	(c), (d) & SF-298's only for (a) & (b)	1
Director, Naval Research Laboratory Attn: Code 5227 4555 Overlook Drive Washington, DC 20375-5326	(a) & (b) w/(SF-298's)	1
Defense Technical Information Center 8725 John J. Kingman Road STE 0944 Ft. Belvoir, VA 22060-6218	(a) & (b) w/(SF-298's)	2
Office of Naval Research Attn: ONR 00CC1 Ballston Centre Tower One 800 North Quincy Street Arlington, VA 22217-5660	(d)	1

cc Mr

If the Program Officer directs, the Grantee shall make additional distribution of technical reports in accordance with a supplemental distribution list provided by the Program Officer. The supplemental distribution list shall not exceed 250 addresses.

* For report types (a) and (b), send only a copy of the transmittal letter to the Administrative Contracting Officer; do not send actual reports to the Administrative Contracting Officer.